LJMU Research Online

Mazzali, PA, Sullivan, M, Pian, E, Greiner, J and Kann, DA

 Spectrum formation in superluminous supernovae (Type I)

http://researchonline.ljmu.ac.uk/id/eprint/7374/

Article

For more information please contact researchonline@ljmu.ac.uk

Spectrum formation in superluminous supernovae (Type I)

P. A. Mazzali,[1,2]★ M. Sullivan,[3] E. Pian,[4,5] J. Greiner[6] and D. A. Kann[7]

[1]*Astrophysics Research Institute, Liverpool John Moores University, IC2, Liverpool Science Park, 146 Brownlow Hill, Liverpool L3 5RF, UK*
[2]*Max-Planck-Institut fr Astrophysik, Karl-Schwarzschild-Str. 1, D-85748 Garching, Germany*
[3]*School of Physics and Astronomy, University of Southampton, Southampton SO17 1BJ, UK*
[4]*Institute of Space Astrophysics and Cosmic Physics, via P. Gobetti 101, I-40129 Bologna, Italy*
[5]*Scuola Normale Superiore, Piazza dei Cavalieri 7, I-56126 Pisa, Italy*
[6]*Max-Planck-Institut fr Extraterrestrische Physik, Giessenbach-Str. 1, D-85748 Garching, Germany*
[7]*Thüringer Landessternwarte Tautenburg, Sternwarte 5, D-07778 Tautenburg, Germany*

ABSTRACT

The near-maximum spectra of most superluminous supernovae (SLSNe) that are not dominated by interaction with a H-rich circum-stellar medium (SLSN-I) are characterized by a blue spectral peak and a series of absorption lines which have been identified as O II. SN 2011kl, associated with the ultra-long gamma-ray burst GRB111209A, also had a blue peak but a featureless optical/ultraviolet (UV) spectrum. Radiation transport methods are used to show that the spectra (not including SN 2007bi, which has a redder spectrum at peak, like ordinary SNe Ic) can be explained by a rather steep density distribution of the ejecta, whose composition appears to be typical of carbon–oxygen cores of massive stars which can have low metal content. If the photospheric velocity is $\sim$10 000–15 000 km s^{-1}, several lines form in the UV. O II lines, however, arise from very highly excited lower levels, which require significant departures from local thermodynamic equilibrium to be populated. These SLSNe are not thought to be powered primarily by ^{56}Ni decay. An appealing scenario is that they are energized by X-rays from the shock driven by a magnetar wind into the SN ejecta. The apparent lack of evolution of line velocity with time that characterizes SLSNe up to about maximum is another argument in favour of the magnetar scenario. The smooth UV continuum of SN 2011kl requires higher ejecta velocities ($\sim$20 000 km s^{-1}): line blanketing leads to an almost featureless spectrum. Helium is observed in some SLSNe after maximum. The high-ionization near-maximum implies that both He and H may be present but not observed at early times. The spectroscopic classification of SLSNe should probably reflect that of SNe Ib/c. Extensive time coverage is required for an accurate classification.

Key words: radiative transfer – techniques: spectroscopic – supernovae: general – supernovae: individual: (SNLS-06D4eu, PTF09cnd, SN 2011kl, iPTF13ajg).

1 INTRODUCTION

Supernovae (SNe) are physically divided into two groups, core-collapse and thermonuclear. Classically, they are typed based on their light curves and spectra (see Filippenko 1997, for a review). Recently, however, new classes of SNe have emerged that only partially fit into this classical scheme. In particular, a number of very luminous events have been detected by different surveys, many at redshifts exceeding 0.5 (e.g. Quimby et al. 2007; Barbary et al. 2009; Chomiuk et al. 2011; Quimby et al. 2011; Leloudas et al. 2012; Howell et al. 2013; Lunnan 2013; Papadopoulos et al. 2015, see Gal-Yam 2012 for a review). Although they are collectively classified as

superluminous supernovae (SLSNe), their observational properties are quite diverse.

Some SLSNe clearly bear the sign of interaction with a hydrogen-rich circum-stellar medium (CSM; Ofek et al. 2007; Smith et al. 2007; Drake et al. 2011; Benetti et al. 2014). This masks the actual SN ejecta, making their nature unclear, although a link with massive stars is likely (e.g. Smith et al. 2007; Agnoletto et al. 2009). SLSNe without the signatures of interaction with a H-rich CSM, ('H-poor SLSNe') are, in turn, divided into two rather vaguely defined groups. Most of them have very blue spectra at maximum which show strong O II lines (SLSN-I; Gal-Yam et al. 2009). Some, such as SN2007bi (Gal-Yam et al. 2009), have different spectra at comparable epochs, closer to those of type Ic SNe (SNe Ic), and are pair-instability SN (PISN) candidates. Both of these latter groups would technically be classified as SNe Ic, or at least as stripped-envelope events, since hydrogen lines are never strong. Finally, the

ULGRB 111209A/SN 2011kl is intermediate in luminosity between GRB/SNe and SLSNe, but its spectral energy distribution resembles that of SLSNe.

Various interpretations have been proposed for these SNe. The PISN candidate SN 2007bi (Gal-Yam et al. 2009) has very extended optical light curves, and emits strong forbidden lines of [Fe II] at late times. This is consistent with a ^{56}Ni-driven light curve, and suggestive of the explosion of a very massive star with a zero-age main-sequence mass close to, or in excess of, 100 $M_\odot$. This scenario has been criticized (e.g. Nicholl et al. 2013), but in our opinion the presence of forbidden emission lines of Fe in an amount compatible with the ^{56}Ni that is necessary to drive the light curve (Gal-Yam et al. 2009) makes the Ni-driven scenario uncontroversial. The massive collapse scenario (Moriya et al. 2010) agrees on this despite uncertainties. For none of the other H-poor SLSNe has the presence or amount of ^{56}Ni been confirmed. These SNe typically show strong absorption lines of lighter elements, including oxygen, and have never been observed in the nebular phase as they are typically too distant to be observed at late times. Their light curves do not appear to be consistent with being powered by ^{56}Ni decay (Inserra et al. 2013; Howell et al. 2013; Papadopoulos et al. 2015). One alternative to ^{56}Ni is that the SN is powered by energy emitted by a magnetized, rapidly spinning neutron star (a Magnetar), (e.g. Bucciantini et al. 2009). In a magnetar-powered scenario, interaction of a magnetar-driven shock with the SN ejecta could transform kinetic energy into radiative energy and power the SN light curve, leading to SLSNe (Kasen & Bildsten 2010; Woosley 2010). Another possibility is interaction with H- and He-free CSM (Chatzopoulos & Wheeler 2012; Moriya & Maeda 2012; Baklanov, Sorokina & Blinnikov 2015; Sorokina et al. 2015). These studies have focused on reproducing the light curves of SLSNe. However, spectra should also be explained. One signature of interaction with an H- and He-free CSM would be shallow absorption lines, and a spectrum that looks too cool for its luminosity, which is the sum of two components, the SN and the interaction. An example is the 'Super-Chandrasekhar' SN Ia 2009dc (Hachinger et al. 2012). This is not what we see in SLSNe. We see the opposite: a spectrum which is too hot for its luminosity. The presence of an outer CSM does not seem to be compatible with the spectra of this class of SLSNe, which we therefore call 'non-interacting'.

Useful information about SN ejecta can be obtained from modelling their spectra. As the SN ejecta expand, deeper and deeper layers of the exploded star are exposed, and spectra reveal their properties. A consistent calculation can be used to determine the abundances in the ejecta, and these in turn may indicate the properties of the progenitor and the effect of the explosion. This has been demonstrated for type Ia SNe (e.g. Mazzali et al. 2008), as well as for SNe Ib/c (e.g. Sauer et al. 2006). However, for SLSNe the only attempts to model the spectra have relied on parametrized codes, which are effective in suggesting line identifications but cannot provide quantitative information with respect to masses, energies and abundances (e.g. Vreeswijk et al. 2014). Here we apply our models to SLSNe. Our methodology is outlined in Section 2.

A variety of SLSN spectra have been presented in various papers (e.g. Chomiuk et al. 2011; Quimby et al. 2011; Inserra et al. 2013; Nicholl et al. 2014; Vreeswijk et al. 2014). Only in a few cases are time series of spectra available. We have selected iPTF13ajg (Section 3) and PTF09cnd (Section 4) as typical examples of line-rich SLSNe. We also examine SNLS-06D4eu (Howell et al. 2013), the most distant spectroscopically confirmed published SLSN to date (Section 5). We then compare the results with a line-poor, luminous SN 2011kl/GRB111209A (Greiner et al. 2015) in Section 6.

We conclude with a discussion of the general properties of SLSN spectra, and the inferences that can be made about these events from their spectral properties (Section 7).

2 METHOD

The spectra of SNe (and SNe Ic in particular) can have lines of different widths. SNe Ic are a particularly interesting case, as the range goes from narrow (a few 1000 km s^{-1}, as for SN 1994I; Sauer et al. 2006) to very broad lines ($\sim$60 000 km s^{-1}, as for SN 2002ap; Mazzali et al. 2002). This is roughly reflected in the classification of SNe Ic versus broad-lined (BL) SNe Ic. Modelling is necessary to turn the intrinsic properties of the gas in the SN ejecta (density and abundance distributions, excitation and ionization degree and their radial dependence) into observed line widths, taking into account the effect of line blending, which is particularly important in the rapidly expanding SN ejecta where the material follows a Hubble-type law.

The spectra of SLSNe are characterized by lines of mostly singly ionized elements, but are unique among SNe in showing O II lines. Line identification, while probably correct especially when multiple features are identified, is often performed using codes that do not treat the level occupation numbers and the radiation field consistently. We therefore need to verify these results. Interestingly, line velocity in SLSNe does not seem to evolve much with time (see e.g. Chomiuk et al. 2011; Nicholl et al. 2014; Vreeswijk et al. 2014). This is different from the typical behaviour of SN spectra. The question is what model can reproduce this.

We modelled the SLSN spectra using our Monte Carlo supernova spectrum synthesis code. This has been described in several papers (Mazzali & Lucy 1993; Mazzali 2000) and has been used to model SNe of different spectral types (Mazzali et al. 2013, 2014a). The code assumes that the SN luminosity is emitted at a lower boundary as a blackbody and transported through an expanding SN 'atmosphere' of variable density and composition. The atmosphere is assumed to be in radiative equilibrium, and radiation can be absorbed in lines or scattered off electrons. Level populations are computed using a modified nebular approximation, which is appropriate for the conditions prevailing in SN ejecta (Pauldrach et al. 1996). The emergent spectrum is computed both by counting emerging energy packets (which are used as proxies for photons), and by solving the formal integral of the transfer equation using as source functions and opacities obtained in the Monte Carlo experiment by iterating with the radiation field (Lucy 1999). Because our code solves for the level populations and the radiation field consistently, it can be used to estimate masses and abundances in the outer part of the SN ejecta (see e.g. Mazzali et al. 2014b).

While the code is not fully self-consistent, in that it does not depend on a specific explosion model but rather uses one to describe the layers above a sharp photosphere, it is also not parametrized, because occupation numbers, and hence line opacities, are computed consistently with the properties of the radiation field. It therefore goes beyond simple line identification, making it possible to quantify relative and absolute elemental abundances simultaneously with the density and mass in the expanding SN ejecta. With the method of abundance tomography (e.g. Stehle et al. 2005) it is possible to take advantage of the progressive thinning out of the SN ejecta and explore the properties of deeper and deeper layers.

The code can treat non-thermal excitation of He consistently, computing the effect on the level population of non-thermal particles as, e.g. produced by radioactive decays (Lucy 1991; Mazzali & Lucy 1998; Hachinger et al. 2012), if the radiation field

is known. This is possible for SNe Ib because we know that the non-thermal radiation field comes from the incomplete thermalization of the gamma-rays and positrons produced by the decay of ^{56}Ni and ^{56}Co. As an alternative, non-thermal effects can be simulated in a parametrized way, modifying the population of the excited levels of relevant ions by introducing departure coefficients that should imitate a consistent calculation (e.g. Mazzali et al. 2009). We use the latter approach here because we do not know the details of the non-thermal radiation field and do not treat non-thermal effects in O II explicitly. However, since the O II ion is characterized by excited levels with a very high-excitation energy, it can be expected to be sensitive to non-thermal radiation in a way similar to He I. We therefore apply departure coefficients similar to those obtained for He I (Lucy 1991; Mazzali & Lucy 1998; Hachinger et al. 2012), mimicking non-thermal effects on O II.

3 LINE-RICH SLSNe: iPTF13ajg

We begin with the spectra of one of the best observed SLSNe, iPTF13ajg, at redshift $z = 0.74$. This supernova was discovered by the intermediate Palomar Transient Factory (iPTF). A large data set for this event was presented in Vreeswijk et al. (2014), making this an excellent 'template' SLSN, since its behaviour is similar to that of many other less well-observed cases. The spectra are characterized by a slow evolution. The strongest lines have been identified as Fe III, C II, C III, Si III, O II (Vreeswijk et al. 2014). The lines are broad, but not extremely broad. A characteristic line width seems to be ~15 000 km s^{-1}. Line blending is not as dominant as in GRB/SNe, for example (see e.g. Iwamoto et al. 1998), or even in non-GRB BL-Ic SNe (e.g. Mazzali et al. 2013). However, line width is not easy to relate to a velocity spread, as most lines are actually blends. Modelling is necessary to address this.

The lines that have been identified are not indicative of a particularly high temperature, despite the high luminosity. This is understandable, because SLSNe evolve slowly in luminosity, and therefore they are observed with much larger radii than SNe Ib/c, which reduces the temperature. The only indication of a very high temperature is the presence of O II lines. It has been noted that the ionization potential of O I is high. While this is true, it is similar to H I (13.6 eV), and much lower than that of He I (24.6 eV). However, this is not the whole story. The observed lines, if they are correctly identified as O II, arise from very highly-excited lower levels, which have excitation potentials of ~25 eV. This is higher than the energy required to excite He I lines in SNe Ib (~20 eV), and indeed comparable to the ionization potential of He I. It is therefore to be expected that the excitation of O II levels is not in thermal equilibrium with the local radiation field. We can test this with our models, and attempt to derive relative abundances in the SN ejecta. This should in turn shed light on the nature of the progenitor and on the mechanism that powers SLSNe.
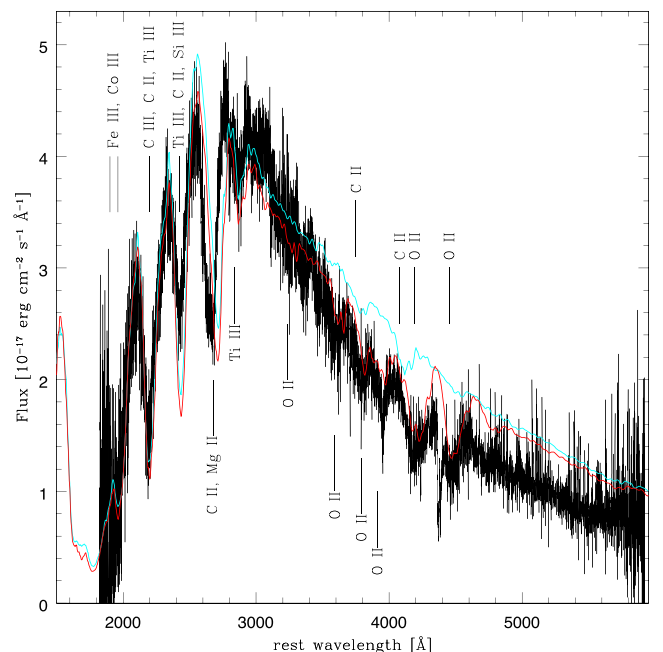
Line velocity evolves very slowly with time in iPTF13ajg, as in other SLSNe. In order for the position of the lines not to move significantly over several weeks or months despite quite a high expansion velocity, either a steady-state situation holds (as in stellar winds), or the density profile must be very steep. In the former case, we would expect very broad lines, since $\rho \propto r^{-2}$, which leads to significant mass being able to absorb radiation over a large range of velocities. Furthermore, the spectra of SLSNe (iPTF13ajg is very well-observed but others show a similar behaviour) are seen to become redder with time as the luminosity evolves. This is typical of SNe and would not be expected in a steady-state regime. We therefore explore the latter option.

In order to reproduce the spectra of iPTF13ajg we used a steep density profile, $\rho \propto r^{-7}$, which is typical of low-energy explosions of compact stars (e.g. Sauer et al. 2006). Line width depends on the gradient of the density (see e.g. Mazzali et al. 2000). Other characteristic features of SLSNe are that they are extremely luminous, but also rather long-lived. In the case of iPTF13ajg the models we tested have ejecta mass ranging from ~25 to ~50 M$_\odot$. The mass is always quite large mass, which is required by the long risetime, the high luminosity and the relatively large velocity (Vreeswijk et al. 2014).

3.1 Pre-maximum epochs

The spectra of PTF13ajg and similar SLSNe before and around maximum light are characterized by strong absorption lines, both in the rest-frame ultraviolet (UV) and in the optical region. The spectra typically turn over at ~2700 Å. This is extremely blue for any SN: normally SN spectra are subject to strong metal absorption (Fe, Co, Ni, Ti, Cr) shortwards of ~4000 Å. The behaviour of SLSNe may indicate a higher temperature than in other SNe Ib/c, but this is in conflict with the ionization degree, which is not extremely high, and with the fact that more highly ionized metal ions are even more likely to absorb in the UV. It seems more likely that it is the result of a low metal abundance.

We focus first on one of the best observed spectra of iPTF13ajg, obtained on 2013 April 9, about 8 d before maximum (Vreeswijk et al. 2014). We adopted a distance modulus $\mu = 43.25$ mag and no reddening. We used a rest-frame epoch of 50 d for this spectrum, starting from the bolometric light curve shown in Vreeswijk et al. (2014, Fig. 5), but we also tested a shorter risetime (40 d). This range of risetimes does not change the nature of our results but does affect the estimate of the mass, as the density profile can be re-scaled down in mass, without altering the ratio between kinetic energy and ejected mass. Fig. 1 shows the spectrum along with two models.

Figure 1. The spectrum of iPTF13ajg on 2013 9 April, compared to two synthetic spectra: one does not include an increase in the occupation numbers of O II and He I to account for non-thermal effects (cyan line), the other does (red line).

Table 1. Parameters of the models for iPTF13ajg.

Date	Epoch (rf d)	Lum (erg s^{-1})	v_{ph} (km s^{-1})	T_B (K)	He	C	O	Ne	Mg	Si	S	Ca	Ti	Fe	Co	Ni
											relative abundances					
2013 April 8	49	44.48	12 250	12 600	0.10	0.40	0.475	0.02	5e-4	2e-3	5e-4	5e-5	2e-5	5e-4	3e-4	1e-5
2013 April 9	50	44.44	12 250	12 100	0.10	0.40	0.475	0.02	5e-4	2e-3	5e-4	5e-5	2e-5	5e-4	3e-4	1e-5
2013 April 16	54	44.48	12 250	11 700	0.10	0.40	0.475	0.02	7e-4	2e-3	5e-4	5e-5	2e-5	5e-4	3e-4	1e-5
2013 May 7	67	44.44	12 250	9800	0.10	0.40	0.475	0.02	5e-4	2e-3	5e-4	5e-5	2e-5	5e-4	3e-4	1e-5
2013 May 10	69	44.44	11 750	9900	0.10	0.40	0.475	0.02	5e-4	2e-3	5e-4	5e-5	1e-5	5e-4	3e-4	1e-5
2013 June 6	84	44.28	11 000	8500	0.10	0.40	0.475	0.02	3e-6	2e-3	5e-4	4e-5	2e-5	5e-4	2e-4	1e-5
2013 June 10	87	44.23	10 750	8200	0.10	0.40	0.475	0.02	1e-5	2e-3	5e-4	4e-5	2e-5	5e-4	2e-4	1e-5
2013 July 12	106	43.81	7500	7900	0.10	0.40	0.475	0.02	3e-6	2e-3	5e-4	4e-5	7e-5	2e-4	8e-5	1e-5
2013 September 9	141	43.58	7000	5400	0.10	0.40	0.475	0.02	1e-5	2e-3	5e-4	4e-5	1e-6	2e-4	1e-4	1e-5

One model was computed without considering non-thermal ionization/excitation, the other includes it in a parametrized way. The models are characterized by the same luminosity (7×10^{10} L$_\odot$), photospheric velocity (12 250 km s^{-1}), and abundances. The photospheric velocity does not evolve much during this phase, and the mass that is responsible for line formation is only ∼3 M$_\odot$. The composition is dominated by carbon (40 per cent by mass), oxygen (48 per cent), helium (10 per cent), neon (2 per cent). Heavier elements have low abundances (see Table 1). The abundances were adjusted to optimize the match to the observed spectrum, and they indicate substantially sub-solar values (∼1/4 solar), based on the iron content.

The thermal model matches the observations reasonably well, but performs best bluewards of 3000 Å. The main contributions to the various lines are marked in Fig. 1, and a list of the strongest lines is presented in Table 2. They are generally in agreement with previous results (e.g. Vreeswijk et al. 2014), but with some differences. In particular, Ti III leaves an important imprint on the spectrum, and it is solely responsible for the line near 2900 Å. In the case of SN 2011kl, this is the only isolated line that is seen (Greiner et al. 2015, see Section 6). In the red part of the spectrum only weak C II lines are produced by this model, which may match some possible observed features but not the strongest lines. These have typically been identified as O II lines.

As mentioned above, all O II lines come from highly excited lower levels. O I itself has an ionization potential of 13.6 eV, like H I and similar to Fe II and Si II. However, all of its near ultra-violet (NUV)-optical lines arise from levels with excitation potential ranging from 23 to 32 eV. Thus, while it is reasonable to expect that O II and Fe III are present, O II lines should not be very strong unless the temperature, and hence the ionization, is even higher. The strength of the O II lines cannot be increased by just increasing the oxygen abundance, as this is already very high.

However, it is possible that the O II levels are excited by non-thermal processes, just like He I lines in SNe Ib (which actually come from lower levels with smaller excitation potentials). We mimicked this by increasing the population of the excited states of O II (and He I) by values comparable to values for SNe Ib (Lucy 1991; Hachinger et al. 2012) and SNe IIb (Mazzali et al. 2009). We applied a single value for each epoch, but the departure coefficient increases with time, from values of ∼100 early on up to ∼10^4 at the later epochs. This reflects the progressive increase of the penetration of non-thermalized particles through the outer ejecta. This is sufficient to produce O II lines that match the observations quite well at rest-frame wavelengths between 3000 and 6000 Å.
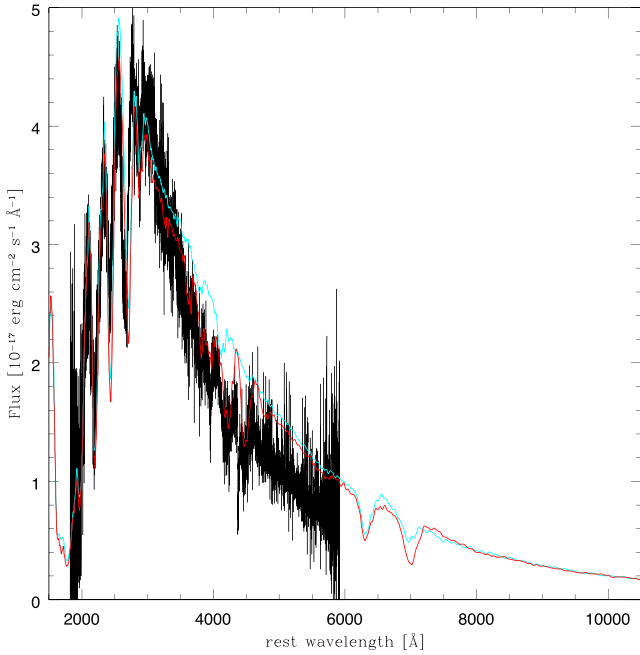
C II lines are quite strong. A C II line (λ4267) is important in shaping the absorption of O II near 4100 Å and making it broad.

Table 2. The strongest lines in the spectra of iPTF13ajg and other similar SLSNe at pre-maximum epochs (the observed λ refers to iPTF13ajg). Lines beyond 6000 Å are predicted by the model.

Feature λ (Å)	Ion	Lab λ (Å)	E_l (eV)
1950	Fe III	2061.56	5.08
	Fe III	2068.25	5.08
	Fe III	2078.99	5.08
	Co III	2097.64	6.91
2200	C III	2296.87	12.69
	C II	2325.40	0.01
	Ti III	2339.00	4.74
2400	C II	2512.06	13.72
	Ti III	2516.07	4.76
	Ti III	2527.85	4.74
	Si II	2541.82	10.28
2670	Mg II	2795.53	0.00
	C II	2836.71	11.96
2830	Ti III	2984.74	5.17
3230	O II	3377.19	25.29
3600	O II	3749.49	23.00
3800	C II	3920.68	16.33
	O II	3954.36	23.42
	O II	3973.26	23.44
3900	O II	4075.86	25.67
4200	C II	4267.26	18.05
	O II	4345.57	22.98
	O II	4349.43	23.00
	O II	4366.91	23.00
	O II	4414.89	23.44
	O II	4416.97	23.42
4450	O II	4638.86	22.97
	O II	4641.83	22.98
	O II	4650.85	22.97
	O II	4661.64	22.98
6250	C II	6578.05	14.45
	C II	6582.88	14.45
	O II	6721.36	23.44
7000	C II	7231.34	16.33
	C II	7236.42	16.33
	O II	7320.66	3.32
	O II	7331.30	3.33

An interesting prediction of this model is that C II 6578 and 7256 Å should be strong (see Fig. 2). This region falls outside the observed optical range for iPTF13ajg. The NIR spectra reported by Vreeswijk et al. (2014) are very noisy.

Figure 2. As Fig. 1, but showing the model prediction in the entire rest-frame optical domain.

The time series of pre-maximum spectra is characterized by an essentially constant photospheric velocity (12 250 km s^{-1}). The luminosity increase leading to maximum light results in a temperature that decreases only slowly as the ejecta expand, which ensures that the spectra show very little sign of change in this period, which covers about one month. This is quite unusual for a SN.
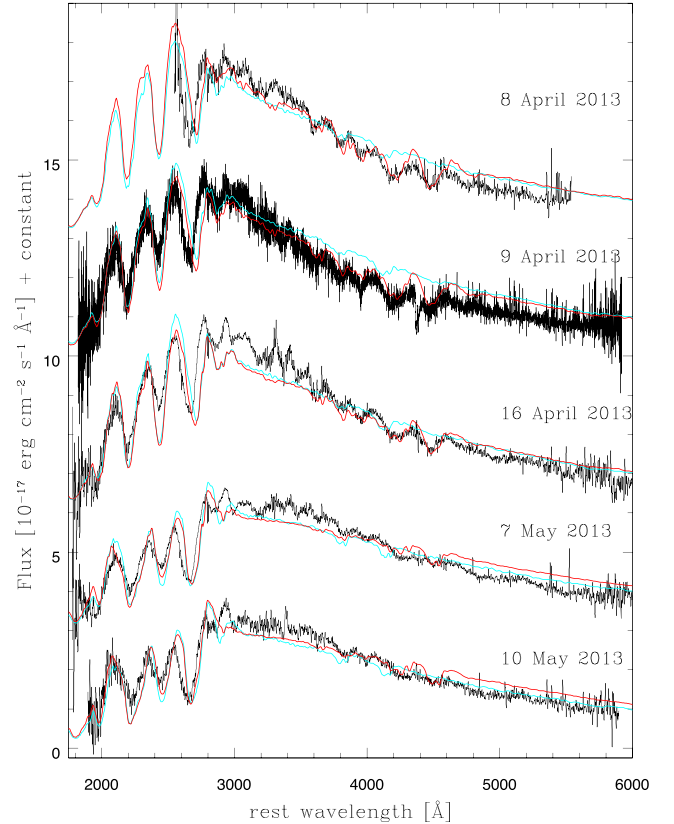
Because of the parametrized treatment of non-thermal processes (we do not know the properties of the non-thermal radiation field, which is unlikely to be the result of partial thermalization of gamma-rays and positrons), we cannot establish the masses of the elements affected with great accuracy. Still, the composition appears to be dominated by helium, carbon and oxygen, the elements that are expected to dominate in the core of a massive star, while heavier elements have sub-solar abundances.

Our density profile has a mass of $\sim$3 M$_\odot$ above the photosphere. Although this produces reasonable conditions in the thermal part of the spectrum, this value should only be taken as indicative. The corresponding kinetic energy of expansion is $\sim$3 $\times$ 10^{52} erg. This is quite large, and is dictated by the need to have a steep gradient in density at velocities of 10–15 000 km s^{-1} in order to guarantee that the photosphere recedes only slowly with time (in practice it corresponds to 3 M$_\odot$ of material moving at 12 000 km s^{-1}). A large mass is also required by the long duration of the light curve. If a shorter risetime is used, a smaller mass and energy are obtained.
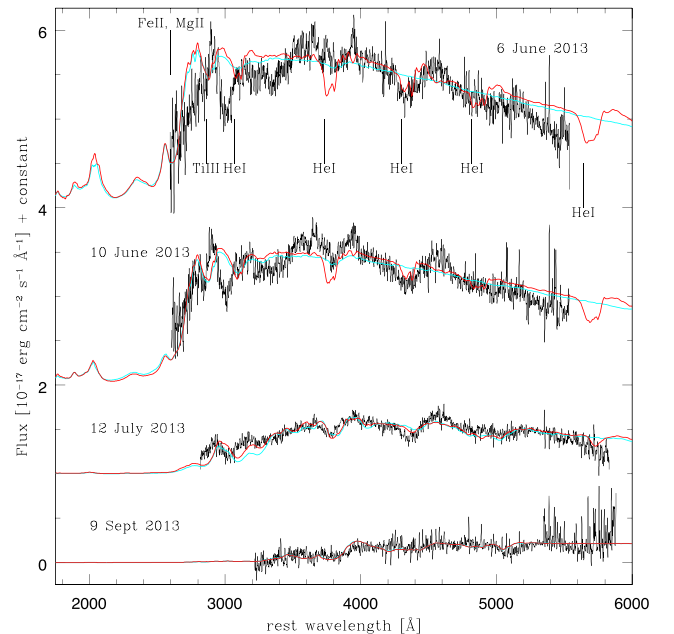
Fig. 3 shows the series of spectra before and near maximum with their corresponding models, both without and with enhanced excitation, to mimic non-thermal effects. The main parameters of all the models are summarized in Table 1.

3.2 Post-maximum epochs

After maximum light, the spectra of iPTF13ajg begin to evolve. The flux peak progressively shifts to the red, which resembles SNe Ib/c. The O II lines are no longer very strong, and lines of lower ionization species become visible. No rest-frame UV information is available, which limits our ability to constrain the metal content in the regions

Figure 3. The pre- and near-maximum spectra of iPTF13ajg, compared to synthetic spectra. One of the model series (cyan) does not include an increase in the occupation numbers of O II and He I to account for non-thermal effects, while the other (red) does.

Figure 4. As Fig. 3, but for the post-maximum spectra of iPTF13ajg.

where the spectra form (see e.g. Mazzali et al. 2014a). Observed and synthetic spectra are compared in Fig. 4.

The decreasing luminosity is now accompanied by a decreasing photospheric velocity, so that the mass above the photosphere

Table 3. Parameters of the models for PTF09cnd.

Date	Epoch (rf d)	Lum (erg s^{-1})	v_{ph} (km s^{-1})	T_B (K)	He	C	O	Ne	Mg	Si	S	Ca	Ti	Fe	Co	Ni
										relative abundances						
2009 August 12	18	43.22	15 250	15 600	0.42	0.10	0.27	0.02	0.08	0.10	5e-4	8e-7	5e-5	6e-5	2e-5	1e-5
2009 August 25	29	43.48	14 200	14 400	0.44	0.11	0.30	0.02	0.06	0.06	6e-4	8e-7	6e-5	7e-5	2e-5	1e-5
2010 February 11	164	43.04	3500	8200	0.46	0.11	0.40	0.02	5e-3	5e-4	5e-4	7e-7	1e-6	1e-4	1e-5	1e-5

becomes quite large at progressively later epochs. We do not require any significant change in the abundances, although the fits are not as good as at pre-maximum epochs (see Fig. 4), and thus we are less confident about these results. He I lines now become visible, and a parametrized increase of the level populations to take non-thermal heating into account is sufficient to reproduce them. This was also used before maximum, but because most He was ionized (He II) He I lines were never strong. Based on its post-maximum spectra, iPTF13ajg should be classified as a SN Ib. It is normal for He I lines to appear late in SNe Ib, as the result of the delayed onset of non-thermal effects on He I in a cool gas caused by the opacity encountered by non-thermalized decay products as they travel in the SN ejecta (Lucy 1991). In the case of iPTF13ajg, however, the late appearance of the He I lines is also due to the late cooling and recombination of He II. On the other hand, the ionization of oxygen is now too low for O II lines ever to become visible.

The synthetic spectra do not match the observed spectra as well as they do at epochs before maximum light. This may partly be the consequence of our ignorance of the flux level in the UV. A strong absorption near 3000 Å is not reproduced. This feature is not often seen in SLSNe, but it seems to be present in LSQS12dlf (Nicholl et al. 2014).

The trend for a cooler spectrum and decreasing velocities continues after maximum. Lines of singly ionized species become more and more dominant as the temperature decreases. Flux blocking in the (unobserved) UV is almost entirely due to iron-group species. At the latest epochs, strong Ca II IR triplet, C I 9062, 9094, and O I 7774 are predicted in the redder part of the visible range, which is also not observed. This is in line with the spectra of other SLSNe (see Nicholl et al. 2014).

As the photospheric velocity decreases with time, we are now exploring deeper regions of the ejecta. Because of the steep density distribution that we adopted, the enclosed mass increases rapidly with depth. In the final model ∼20 M$_\odot$ of material contribute to the spectrum. This is necessary because at an epoch of ∼140 d the spectra still show significant absorption.
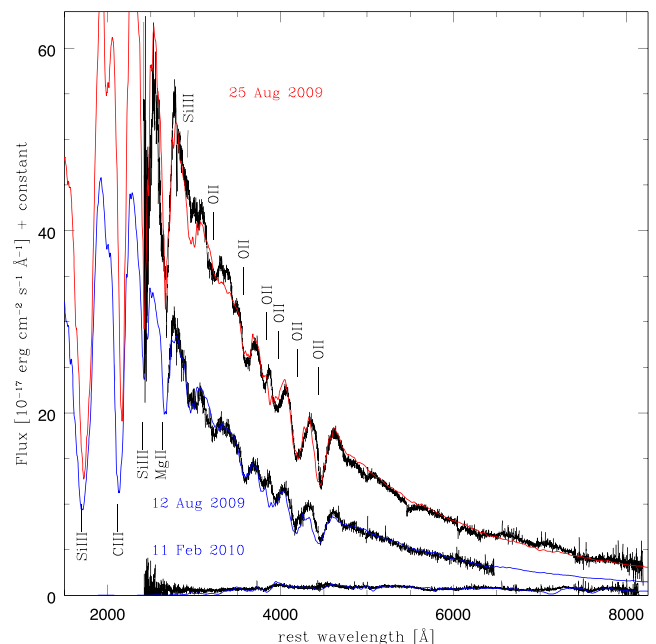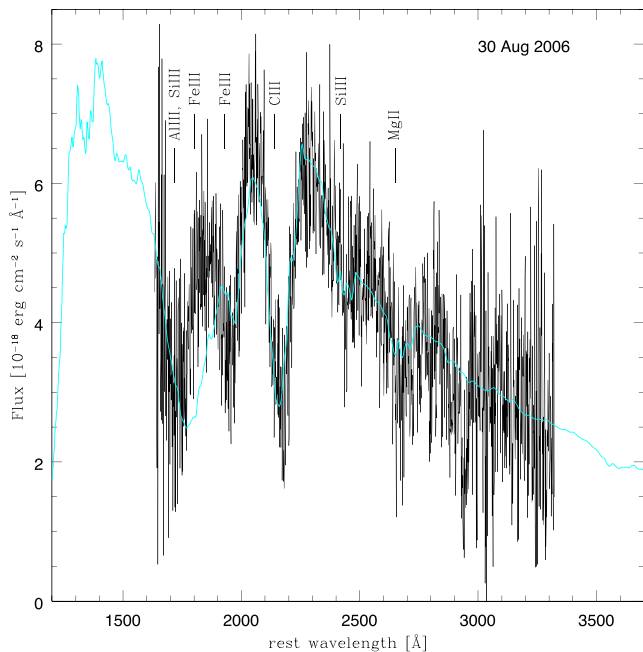
4 LINE-RICH SLSNe: PTF09cnd

The SLSN PTF09cnd (Quimby et al. 2011), discovered by the Palomar Transient Factory (PTF), has coverage of both the pre-and post-maximum epochs. We use the original classification spectrum taken at the 4.2-m William Herschel Telescope (WHT) with the Intermediate dispersion Spectrograph and Imaging System (ISIS), as well as two later spectra taken at the 10-m Keck-I telescope with the Low Resolution Imaging Spectrograph (see Quimby et al. 2011, for details on the spectra). Because of the relatively low redshift ($z = 0.258$), data only cover the UV redwards of 2500 Å. PTF09cnd was significantly less luminous than iPTF13ajg, and reached maximum more rapidly, but its spectra resemble those of iPTF13ajg, showing the O II line series in the optical prior to maximum and a few strong metal lines in the only partially observed NUV. The combination of lower luminosities and smaller epochs leads to a similar spec-

tra evolution. In the final spectrum, He I lines are strong, so that PTF09cnd would also be classified as a SN Ib.

We modelled PTF09cnd with the same background structure as iPTF13ajg, including non-thermal excitation. A distance modulus $\mu = 40.55$ mag was used. The two August spectra are both before maximum, which occurred towards the end of August. Despite the lower luminosity, our fits indicate that the spectra are shaped by the same lines which were identified in iPTF13ajg, although the UV is only partially explored. The spectra can be reproduced using a smaller mass (7–15 M$_\odot$), such that the pre-maximum spectra are shaped by only ∼0.5 M$_\odot$ of ejecta. As we mentioned above, the total mass cannot be determined with great accuracy in the absence of nebular spectra. The mass above the photosphere is subject to uncertainties in our estimated date of explosion and non-thermal departure coefficients. The kinetic energy is 7–15 10^{51} erg. The main results are reported in Table 3. Synthetic spectra are compared to the observed ones in Fig. 5. In the figure, spectra are shown with their real flux level. Because of the very rapid rise to maximum, the temperature in the earlier spectra is actually higher than in iPTF13ajg. The spectra before maximum show very little evolution. The line velocity also remains practically constant. Only much later, in the post-maximum phase, do spectra turn red. At this point, non-thermally excited O II lines are no longer visible.

Because of the limited UV coverage the determination of the metal content is less reliable, but results seem to indicate a low metallicity, as in iPTF13ajg or lower. One significant difference is the weakness of the C II lines: the lines between 3000 and 4000 Å are weak, while those between 6000 and 7000 Å are absent. Although

Figure 5. The spectra of PTF09cnd (black), compared to synthetic spectra.

Figure 6. The near-maximum light spectrum of SNLS-06D4eu (black), compared to a synthetic spectrum (blue).

this is partly due to the higher temperature, which almost completely suppresses C II, we still need to use a significantly lower abundance than in iPTF13ajg. This is also useful to keep several UV lines, and in particular the one near 2200 Å, which is dominated by C III 2297 Å, from becoming too strong, creating too much fluorescent flux to the red. We also need a much lower Fe abundance than in iPTF13ajg, again in order to prevent very strong UV lines. None of these lines are covered by the spectra, so these estimates are highly uncertain.

5 LINE-RICH SLSNe: SNLS-06D4eu

The final line-rich SLSN that we consider is SNLS-06D4eu, the furthest spectroscopically confirmed SLSN at the time of writing. The event was discovered by the Supernova Legacy Survey (SNLS; Perrett et al. 2010) at a redshift $z = 1.588$ (Howell et al. 2013), confirmed using the European Southern Observatory Very Large Telescope with the FORS1 instrument. It has a similar luminosity as iPTF13ajg. Because of the high redshift, the ground-based spectrum only samples the rest-frame UV, reaching very short wavelengths. Since the SN was optically faint and it was not spectrally identified at the time of observation, only one spectrum is available, at an epoch close to maximum. This is shown in Fig. 6 together with a synthetic spectrum computed using a distance modulus $\mu = 45.34$ mag.

The model that was used to compute the synthetic spectrum was again the same as in the previous cases. The SN rose to peak relatively rapidly, so that the epoch of spectrum is estimated to be only about 14 rest-frame days after explosion. This indicates a relatively low mass, and so we used the same mass as for PTF09cnd ($\sim 15 \, M_\odot$). The rapid rise and the high luminosity require a high velocity in order for the temperature and the ionization to reach the observed values. SNLS-06D4eu has the highest velocity of any of the line-rich SLSNe analysed here. Only the GRB/SN 2011kl reaches higher velocities (see next section). We used $v \sim 16\,500 \, \text{km s}^{-1}$, yielding a temperature near the photosphere of $\sim 18\,000$ K, the highest temperature of any of the spectra modelled in this paper. The

mass above the photosphere is only slightly less than in the case of PTF09cnd. The high temperature causes the spectrum to have an even bluer turnover (near 2000 Å) than previous cases (~ 2800 Å). Only $\sim 0.25 \, M_\odot$ of material contribute to the spectrum. Model parameters are given in Table 4.

Beyond 2000 Å, the spectrum is similar to those of other SLSNe, showing lines of C III, Fe III, Si III, Mg II. The line near 2200 Å can be reproduced as C III 2297 Å, but a very low carbon abundance is required to reproduce the line strength, even lower than in the case of PTF09cnd. C II lines are very weak in both PTF09cnd and SNLS-06D4eu, because the average ionization is much higher than what would favour the formation of these lines. This is a consequence of the high temperature. The lack of C II lines may indeed be a common feature of SLSNe at very early epochs. At the same time, a high iron abundance is needed to reproduce the feature near 1800 Å as Fe III. This is in contrast with our model for PTF09cnd. If this is correct, this suggests that the ejecta of SNLS-06D4eu were nuclearly processed, so that it is not possible to determine a metallicity. Silicon also has a high abundance, as indicated by the strength of the line near 2400 Å, which is reproduced as Si III 2542 Å, although the dominant ionization stage of silicon is Si IV.

Bluewards of 2000 Å, Fe III lines are important, but the strong absorption near 1800 Å does not seem compatible with Fe III. It is better reproduced by the resonance line Al III 1854 Å. This line is normally seen in the spectra of late-O stars (Walborn, Nichols-Bohlin & Panek 1985) as well as in B-stars (Rountree & Sonneborn 1993), including interacting binaries (Mazzali 1987; Mazzali et al. 1992). It has not – to our knowledge – been individually resolved in Type I SN spectra, as line blocking by Fe lines is usually too strong (Mazzali & Lucy 1990, identified this line in the spectrum of SN 1987A). The resonance line Si III 1892 Å also contributes to this line. Many lines of doubly ionized ions are visible; the singly ionized species are weak due to the high temperature. It should be noted that Fe III lines do not have the same predicted ratio in the synthetic spectrum as the observed features. In particular, the synthetic absorption near 1700 Å appears too red because it is affected by Fe III 1895, 1914, 1926 Å, which is necessary in order to form the line near 1950 Å, which is Fe III 2068, 2079 Å. The Mg II resonance line (2795, 2805 Å) is visible near 2600 Å but is weak, while Si III 2542 is responsible for the weak absorption near 2400 Å.

Since the spectra do not cover the rest-frame optical, we cannot determine whether O II lines are as strong as in other SLSNe. However, the higher ionization degree of this spectrum means that strong non-thermal effects are not required to cause the O II lines to appear.

6 LINE-POOR SLSNe: GRB/SN 2011kl

While most known SLSNe show similar spectra, recently a SN has been discovered in association with an ultra-long gamma-ray burst (ULGRB), GRB111209A at a redshift $z = 0.67$. The SN shows many characteristics of SLSNe. SN 2011kl was much more luminous than classical GRB/SNe, but was not quite as luminous as SLSNe (Greiner et al. 2015). Its light curve evolved over just a few weeks, as do GRB/SNe, but its spectrum (available only near maximum) did not show any of the broad lines that characterize GRB/SNe (see e.g. Iwamoto et al. 1998) or BL SNe Ic (see e.g. Mazzali et al. 2013). The spectrum was blue, turning over only at ~ 3000 Å, like SLSNe. Unlike SLSNe, it was rather featureless, with only one strong and rather broad absorption line, near 2800 Å.

In Greiner et al. (2015), we adopted a model similar to the one used here to reproduce the spectrum of SN2011 kl. Here we
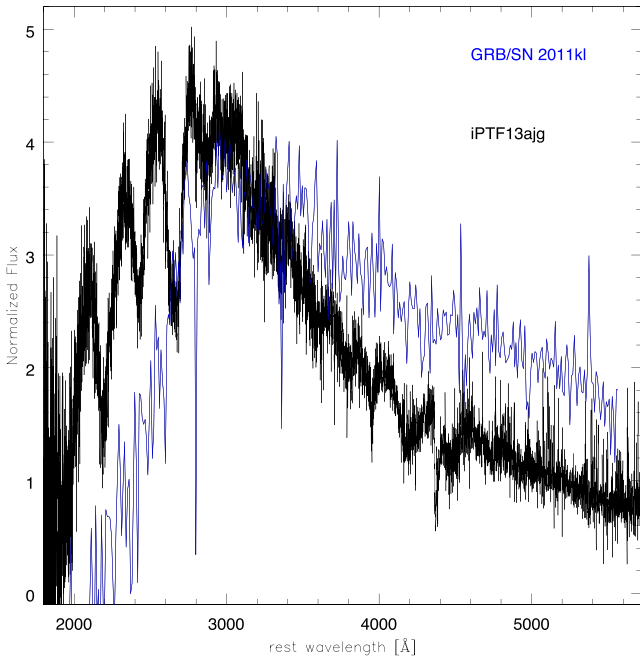
Table 4. Parameters of the models for SNLS-06D4eu.

Date	Epoch (rf d)	Lum (erg s^{-1})	v_{ph} (km s^{-1})	T_B (K)	He	C	O	Ne	Mg	Al	Si	S	Ca	Ti	Fe	Co	Ni
2006 August 31	14	44.32	16500	18200	0.30	2e-3	0.43	0.02	0.10	2e-4	0.12	0.02	1e-5	5e-5	6e-3	1e-4	4e-5

Table 5. Parameters of the models for GRB/SN.

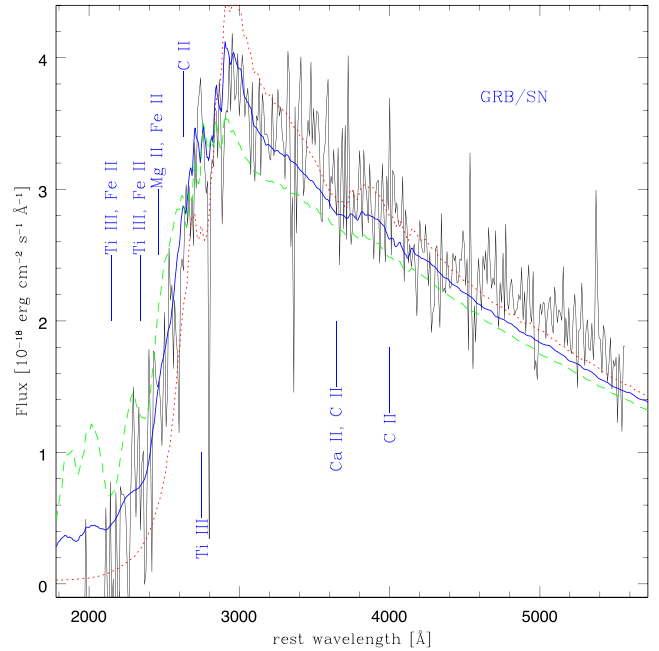| Date	Epoch (rf d)	Lum (erg s^{-1})	v_{ph} (km s^{-1})	T_B (K)	He	C	O	Ne	Mg	Si	S	Ca	Ti	Fe	Co	Ni
2011 December 29	12	43.37	19 500	10 000	0.14	0.30	0.53	0.02	5e-5	0.01	5e-3	2e-4	1e-4	6e-4	1e-4	1e-5

Figure 7. The maximum-light spectrum of GRB/SN 2011kl (blue line) compared to that of iPF13ajg (black line).

Figure 8. The maximum-light spectrum of GRB/SN 2011kl compared to synthetic spectra. The blue (solid) line shows a model with metallicity $Z \sim 1/4\,Z_\odot$. The red (dotted) line shows a model with metallicity reduced by a factor of 3 ($Z \sim 1/12\,Z_\odot$). The green (dashed) line shows a model with metallicity increased by a factor of 3 ($Z \sim 3/4\,Z_\odot$). The strong narrow absorption line near 2800 Å is the Mg II resonance line from the host galaxy.

highlight some of the features of that model, and contrast them to those of SLSNe. A distance modulus $\mu = 43.01$ mag was used. Model parameters are given in Table 5.

In Fig. 7, we compare the spectrum of SN 2011kl with that of iPTF13ajg. The similarity is clear. If the line seen near 2900 Å is that same as the line which is identified as Ti III in iPTF13ajg, then the velocity must be higher in SN 2011kl, as the blueshift is larger. We adopted for SN 2011kl a similar density distribution as for iPTF13ajg, but set a photospheric velocity of $\sim$20 000 km s^{-1}, as opposed to $\sim$12 000 km s^{-1}.

The spectrum of SN 2011kl appears somewhat cooler, which is the result of the lower luminosity and the higher expansion velocity. The high photospheric velocity means that line blending is stronger in SN 2011kl. Line blending is particularly strong in the UV, where many lines are present which merge causing significant line blanketing. This is seen also in GRB/SNe, which are characterized by a high velocity. The metal content is quite similar in the two events. The spectrum does not show strong O II lines, suggesting that non-thermal effects are not strong in SN 2011kl.

In order to set the level of the UV flux, the mass above the photosphere and the abundance of metals can be adjusted. We find that a mass of $\sim$0.3 M$_\odot$ above 19 000 km s^{-1} leads to the best con-

vergence. Since only one spectrum is available, it is not possible to determine whether the density profile is the same at lower velocities. The rapid evolution of the light curve however suggests a smaller mass ($\sim$2.5 M$_\odot$; Greiner et al. 2015), and a higher ratio of kinetic energy to ejected mass. This is similar to the case of GRB/SNe when compared to normal Type Ib/c SNe. Keeping the composition similar to the model of iPTF13ajg, and modifying only the ratio of metals versus carbon and oxygen, we find that a metal content of $\sim$1/4 solar is required for SN 2011 kl, which is in line with the metallicity estimated for the host galaxy (Greiner et al. 2015). Additionally, the temperature is lower because of the lower luminosity. Line blanketing and the lower temperature depress the UV spectrum shortwards of 3000 Å compared to iPTF13ajg 7. Our synthetic spectrum is compared to the observed one in Fig. 8.

We tested different metal abundances by modifying the abundances of all elements heavier than Neon. The results are shown in 7. At lower metal content line blending is reduced and some of the individual line features begin to appear. Also, the UV flux shortwards of 3000 Å is too high, so less radiation is reprocessed to the

Table 6. Inferred ejecta masses and energies of SLSNe.

SN	Mass ($M_\odot$)	E_K (erg)
iPTF13ajg	25–50	2.5–5.0×10^{52}
PTF09cnd	7–15	7–15×10^{51}
SNLS-06D4eu	7–15	7–15×10^{51}
SN 2011kl	2–3	5–8×10^{51}

red and the flux above 3000 Å is too low. Conversely, if the metal content is too high, the flux shortwards of 3000 Å is suppressed, and the excessive reprocessing least to a strong peak near 3000 Å.

Interestingly, the metallicity used for SN 2011kl is similar to that in iPTF13ajg. Several papers on SLSNe estimated the star formation rate in the host galaxy, while it is less common to find an estimate of the metallicity. In the case of SN 2006oz, Leloudas et al. (2012) quote a value $Z/Z_\odot \sim 0.17^{+0.18}_{-0.08}$, which is in line with our estimates in SLSNe. So our models may be used to estimate the metallicity of the progenitor, as in the case of other SNe (Mazzali et al. 2014a).

7 DISCUSSION

Our models show that the spectra of SLSNe can be reproduced almost self-consistently by making just a few assumptions, which are necessary to reproduce some of the peculiar features of these spectra. These observed features and their implications are listed below.

(i) The spectral lines do not evolve in velocity until well after maximum: this requires a steep density gradient, such that the decrease in density with radius is faster than that with time. We adopted a density structure characterized by $\rho \propto r^{-7}$. This is typical of low-energy 1D explosions of compact progenitors (e.g. Sauer et al. 2006), but is not normally seen in high-energy SNe Ib/c, and it may suggest that SLSNe are overall more spherically symmetric than SNe Ib/c with a high E_K/M_{ej} (Leloudas et al. 2015). SLSNe seem to have a low $E_K/M_{ej} \sim 1$ [10^{51} erg $M_\odot^{-1}$], as shown in Table 6.

(ii) The line velocities are not particularly high. This can be simulated by adjusting the density. The steep density profile also means that the lines are not very broad.

(iii) The light curves of many SLSNe are broad. This requires a large ejected mass, independent of the powering mechanism.

(iv) Spectral lines from very highly excited states are observed. Even at the high luminosities of SLSNe, lines such as O II, which are strong in the optical before maximum, require non-thermal excitation processes. He I lines are affected as well, but only appear at later epochs, when the temperature is lower and He is not mostly He II.

(v) The metal lines are weak, and the spectra are blue. This requires a fairly low metal abundance. In the ase of iPTF13ajg, we find a metallicity of ~1/4 solar. This only produces weak iron lines, and allows the spectrum to turn over at ~3000 Å, compared to ~4000 Å in other SNe Ib/c. SN 2011kl has a similar metallicity, but line blanketing depresses the UV flux shortwards of ~3000 Å.

(vi) The composition of the ejecta that contribute to spectrum formation is consistent with the CO cores of massive stars, indicating a common origin of SNe Ib/c and SLSNe. The latter appear to have larger masses on average, but it may well be that such events are rare and only the brightest end has been uncovered so far. The case of the GRB/SN 2011kl, which was not as luminous as the rest of the SLSNe but was discovered only thanks to the GRB, indicates

that this may indeed be the case. SNLS-06D4eu may show signs of nuclearly processed material.

(vii) The fact that the spectrum can be reproduced using the full SN luminosity including the depth of the lines suggests that these SNe are not energized by interaction with an external H- and He-poor CSM.

While these are general results, it is difficult to be precise about the mass and energy of the explosion. Our models (see Table 6) require large masses, but do not explore the inner layers because there are no very late-time data. Therefore the mass values given in Table 6 should be regarded as estimates only. The kinetic energy of our models range from 0.4 to ~5 × 10^{52} erg. This range is typical of GRB/SNe. The ratio E_K/M_{ej} is not far from 1 [10^{51} erg $M_\odot^{-1}$], ensuring that lines are not too broad, except for GRB/SN 2011kl, which reaches $E_K/M_{ej} \approx 2$ and has blended lines. Determining the mass of the inner region has to rely on parametrized fits of the light curve, as we do not have nebular spectra. This has been done in many papers (e.g. Nicholl et al. 2015). Considering the uncertainties (risetime, structure of the inner ejecta), results are in general agreement with ours.

Finally, are normal SNe Ib/c, GRB/SNe, ULGRB/SNe and SLSNe related? They probably all originate from stripped cores of massive stars. In the case of SNe Ib/c, the light curve is dominated by ^{56}Ni, and the energy seems to be proportional to the mass and the ^{56}Ni mass (Mazzali et al. 2013). The inferred progenitor mass rarely exceeds 25 $M_\odot$. They may be classical neutrino-driven explosions, although the increased ^{56}Ni mass and E_K may suggest an additional contribution to the energetics of the event, such as the increasing impact of a magnetar (Mazzali et al. 2006). GRB/SNe are more massive (35–50 $M_\odot$), produce more ^{56}Ni, but are also much more energetic. While the collapsar mechanism is a serious possibility (MacFadyen & Woosley 1999), the fact that all well-studied GRB/SNe are very similar and that the E_K is very nearly constant and close to 2 × 10^{52} erg, the limiting energy of a magnetized neutron star, suggests that magnetar energy may be the driving mechanism (Mazzali et al. 2014b). In this case, magnetar energy would need to be applied very early on, so that it could contribute to nucleosynthesis as well as to energizing the explosion. In the case of the ULGRB/SN, the GRB was so long that it may not be compatible with typically assumed black hole accretion rates in the Collapsar mechanism (Woosley 1993; MacFadyen & Woosley 1999; MacFadyen, Woosley & Heger 2001) unless a very large mass is accreted. Thus, the magnetar energy injection scenario may be an appealing alternative. Finally, for classical SLSNe, the constancy of the line velocity as well as the very large luminosity suggests again that magnetar energy plays a major role in shaping the SN ejecta. In this case, magnetar energy may not be injected immediately and may not contribute to nucleosynthesis, although it may add E_K. The E_K deduced from our models is again in line with the maximum magnetar energy. The delayed addition of magnetar energy may shock the SN ejecta and produce X-rays which then give rise to the non-thermal spectrum and the optical radiation which sustains the light curve for a much longer time than GRB/SNe. This process may also lead to the steep density profile which is needed for the stationary lines, although this may just be explained if the explosion was spherically symmetric, in which case magnetar energy would act like a 'piston'. Part of the reason for the extended light curve of SLSNe is also the large mass of the SN ejecta.

The spectroscopic properties of non-interacting SLSNe reflect those of SNe Ib/c. Although near peak, most non-interacting SLSNe would be classified as type Ic, He lines often appear after

maximum, when the temperature drops, so they should be re-classified as SNe Ib. The reason for the late appearance of the He lines is however different in the two cases: in normal SNe Ib non-thermal effects populating the excited levels of He I above their thermal values can only happen late, when non-thermal particles can penetrate through the ejecta and deposit their energy in the He layer. In SLSNe, on the other hand, the temperature near maximum, when non-thermal effects are important for O II, is too high for He I lines, which become strong when He starts to recombine. When they finally appear, He I lines are also subject to non-thermal excitation effects.

This leads us to making another comment: if hydrogen was present in SLSNe, it would most likely not be visible near maximum because it would be almost completely ionized. The lack of observed H lines near maximum in SLSNe suggests that any H content should not be very large. SLSNe with a lot of H may belong to the interacting class (similar to SNe IIn), while SLSNe of type IIP may not exist because the progenitors of SLSNe may be too massive to retain the H envelope. However, it would not be surprising to see SLSNe showing H lines as they cool down after maximum. These would then formally be 'SLSN-IIb', making the 'Type I' classification inaccurate. H has recently been observed to be present very close to the SN (Yan et al. 2015). It seems therefore dangerous to classify SLSNe as stripped-envelope subtypes, or even as 'Type I' or H-poor, as long as we do not have a more complete temporal coverage of their properties. We have adopted the definition SLSN-I in this paper for clarity, but we think this is not a fully appropriate definition. We do however believe that non-interacting SLSNe share the same properties as stripped-envelope SN, as suggested by Pastorello et al. (2010).

On the other hand, GRB production seems to be agnostic about whether the stellar explosion turns out to be a SN Ib/c or a SLSN. If GRBs are beamed, we should expect to find 2011kl-like SLSN without a GRB. SN 2011kl was less luminous than 'normal' SLSNe, so such events may not have been discovered yet because they are rare and too faint to be discovered optically at their typically large distances. We also should expect that there is no discontinuity in luminosity between SN 2011kl and 'typical' SLSNe.

SLSNe are so luminous that they are unlikely to be driven by ^{56}Ni, but at the same time it is diffcult to determine just how much ^{56}Ni they contain. If a SLSN synthesized as much ^{56}Ni as a GRB/SN, this would go almost unnoticed because the light curve is a lot brighter. It may be expected that, if and when the contribution of whatever alternative power source fades, the SN may fall back on the ^{56}Ni light curve, as was the case for SN 2005bf (Maeda et al. 2007). Apart from this particular case, this has never been observed, possibly because it is difficult to follow SLSNe for a very long time. Magnetar solutions predict a different late-time behaviour than ^{56}Ni solutions (see e.g. Greiner et al. 2015), so it is possible that the real ^{56}Ni contribution remains hidden for a long time. Interaction with an outside CSM, on the other hand, should terminate at some point, and the light curve fade rapidly. The fact that this has not been observed is another argument against the outer CSM scenario. Very late-time observations may shed light on this, as they did in the case of the pair-instability candidate SN 2007bi (Gal-Yam et al. 2009), where the emission in Fe lines matches the expectations for the ^{56}Ni content required to power the peak of the light curve. An additional reason to think that SN 2007bi and similar events are not magnetar-driven SLSNe is the lack of the O II line series despite the O-rich composition, which suggest lack of a strong X-ray flux despite the large oxygen mass inferred from the nebular spectra. Since SN 2007bi was O-rich, this means that

X-rays from ^{56}Ni should be less powerful than X-rays from the shock.

We therefore may have a situation where prompt magnetar energy injection may produce nucleosynthesis in GRB/SN and help drive the explosion. If the energy is injected later, as would be the case for a lower magnetic field, it would not contribute to nucleosynthesis, but it may be converted into radiative energy. This may be the case for SLSNe, but also for SN 2005bf (Tominaga et al. 2005; Maeda et al. 2007), which was the result of the explosion of a less massive star. The late excitation of the He I lines in this case may well be a consequence of the injection of X-rays from interaction with a magnetar wind, since the mass of ^{56}Ni synthesized was not very large (Maeda et al. 2007). It cannot be ruled out that SLSNe commonly host ULGRBs. In this case, the presence of a He shell would probably not constitute a problem for the propagation of the jet, because the engine is active for a very long time.

On the other hand, non-interacting SLSNe may be divided in magnetar-driven and ^{56}Ni-driven, and the latter may be identified as PISN or massive and energetic core-collapses (Moriya et al. 2010). The presence or lack of the O II line series may be a way to discriminate between them, as are the behaviour of the light curve and the late-time spectrum.

ACKNOWLEDGEMENTS

REFERENCES

Agnoletto I. et al., 2009, ApJ, 691, 1348
Baklanov P. V., Sorokina E. I., Blinnikov S. I., 2015, Astron. Lett., 41, 95
Barbary K. et al., 2009, ApJ, 690, 1358
Benetti S. et al., 2014, MNRAS, 441, 289
Bucciantini N., Quataert E., Metzger B. D., Thompson T. A., Arons J., Del Zanna L., 2009, MNRAS, 396, 2038
Chatzopoulos E., Wheeler J. C., 2012, ApJ, 760, 154
Chomiuk L. et al., 2011, ApJ, 743, 114
Drake A. J. et al., 2011, ApJ, 735, 2
Filippenko A. V., 1997, ARA&A, 35, 309
Gal-Yam A., 2012, Science, 337, 927
Gal-Yam A. et al., 2009, Nature, 462, 624
Greiner J. et al., 2015, Nature, 523, 189
Hachinger S., Mazzali P. A., Taubenberger S., Hillebrandt W., Nomoto K., Sauer D. N., 2012, MNRAS, 422, 70
Howell D. A. et al., 2013, ApJ, 779, 98
Inserra C. et al., 2013, ApJ, 770, 128
Iwamoto K. et al., 1998, Nature, 395, 672
Kasen D., Bildsten L., 2010, ApJ, 717, 245
Leloudas G. et al., 2012, A&A, 541, A129
Leloudas G. et al., 2015, ApJ, 815, L10
Lucy L. B., 1991, ApJ, 383, 308
Lucy L. B., 1999, A&A, 345, 211
Lunnan R. et al., 2013, MNRAS, 771, 97
MacFadyen A. I., Woosley S. E., 1999, ApJ, 524, 262
MacFadyen A. I., Woosley S. E., Heger A., 2001, ApJ, 550, 410
Maeda K. et al., 2007, ApJ, 666, 1069
Mazzali P. A., 1987, ApJS, 65, 695
Mazzali P. A., 2000, A&A, 363, 705

Mazzali P. A., Lucy L. B., 1990, in Rolfe E. J., ed., ESA SP-310, Evolution in Astrophysics: IUE Astronomy in the Era of New Space Missions. ESA, Noordwijk, p. 483

Mazzali P. A., Lucy L. B., 1993, A&A, 279, 447

Mazzali P. A., Lucy L. B., 1998, MNRAS, 295, 428

Mazzali P. A., Pauldrach A. W. A., Puls J., Plavec M. J., 1992, A&A, 254, 241

Mazzali P. A. et al., 2000, ApJ, 545, 487

Mazzali P. A. et al., 2002, ApJ, 572, L61

Mazzali P. A. et al., 2006, Nature, 442, 1018

Mazzali P. A., Sauer D. N., Pastorello A., Benetti S., Hillebrandt W., 2008, MNRAS, 386, 1897

Mazzali P. A., Deng J., Hamuy M., Nomoto K., 2009, ApJ, 703, 1624

Mazzali P. A., Walker E. S., Pian E., Tanaka M., Corsi A., Hattori T., Gal-Yam A., 2013, MNRAS, 432, 2463

Mazzali P. A. et al., 2014a, MNRAS, 439, 1959

Mazzali P. A., McFadyen A. I., Woosley S. E., Pian E., Tanaka M., 2014b, MNRAS, 443, 67

Moriya T., Maeda K., 2012, ApJ, 756, L22

Moriya T., Tominaga N., Tanaka M., Maeda K., Nomoto K., 2010, ApJ, 717, L83

Nicholl M. et al., 2013, Nature, 502, 346

Nicholl M. et al., 2014, MNRAS, 444, 2096

Nicholl M. et al., 2015, MNRAS, 452, 3869

Ofek E. et al., 2007, ApJ, 659, L13

Papadopoulos A. et al., 2015, MNRAS, 449, 1215

Pastorello A. et al., 2010, ApJ, 724, L16

Pauldrach A. W. A., Duschinger M., Mazzali P. A., Puls J., Lennon M., Miller D. L., 1996, A&A, 312, 525

Perrett K. et al., 2010, AJ, 140, 518

Quimby R., Höflich P., Akerlof C. W., Rykoff E. S., 2007, ApJ, 668, 99

Quimby R. et al., 2011, Nature, 474, 487

Rountree J., Sonneborn G., 1993, NASA Reference Publication, 1312

Sauer D. N., Mazzali P. A., Deng J., Valenti S., Nomoto K., Filippenko A. V., 2006, MNRAS, 369, 1939

Smith N. et al., 2007, ApJ, 666, 1116

Sorokina E. et al., 2015, preprint (arXiv:1510.00834)

Stehle M., Mazzali P. A., Benetti S., Hillebrandt W., 2005, MNRAS, 360, 1231

Tominaga N. et al., 2005, ApJ, 633, L97

Vreeswijk P. et al., 2014, ApJ

Walborn N. R., Nichols-Bohlin J., Panek R. J., 1985, in Walborn N. R., Nichols-Bohlin J., Panek R. J., Mead J. M., eds, International Ultraviolet Explorer Atlas of O-type Spectra from 1200 to 1900 Å. NASA Reference Publication, 1155

Woosley S. E., 1993, ApJ, 405, 273

Woosley S. E., 2010, ApJ, 719, L204

Yan L. et al., 2015, ApJ, 814, 108

SUPPORTING INFORMATION

Additional Supporting Information may be found in the online version of this article:

XSspectracomp_referee.eps

(http://mnras.oxfordjournals.org/lookup/suppl/doi:10.1093/mnras/stw512/-/DC1).

Please note: Oxford University Press are not responsible for the content or functionality of any supporting materials supplied by the authors. Any queries (other than missing material) should be directed to the corresponding author for the article.

This paper has been typeset from a TEX/LATEX file prepared by the author.